

Anchor-free Cross-view Object Geo-localization with Gaussian Position Encoding and Cross-view Association

Xingtao Ling, Chenlin Fu, Yingying Zhu*

College of Computer Science and Software Engineering, Shenzhen University, China
zhuyy@szu.edu.cn

Abstract

Most existing cross-view object geo-localization approaches adopt anchor-based paradigm. Although effective, such methods are inherently constrained by predefined anchors. To eliminate this dependency, we first propose an anchor-free formulation for cross-view object geo-localization, termed AFGeo. AFGeo directly predicts the four directional offsets (left, right, top, bottom) to the ground-truth box for each pixel, thereby localizing the object without any predefined anchors. To obtain a more robust spatial prior, AFGeo incorporates Gaussian Position Encoding (GPE) to model the click point in the query image, mitigating the uncertainty of object position that challenges object localization in cross-view scenarios. In addition, AFGeo incorporates a Cross-view Object Association Module (CVOAM) that relates the same object and its surrounding context across viewpoints, enabling reliable localization under large cross-view appearance gaps. By adopting an anchor-free localization paradigm that integrates GPE and CVOAM with minimal parameter overhead, our model is both lightweight and computationally efficient, achieving state-of-the-art performance on benchmark datasets.

Introduction

Consider Fig. 1 (a): if we know the location of an object of interest in the query image, how can we find that object in the reference image with known geographic information to obtain the object’s geographic coordinates? Addressing this question is the goal of cross-view object geo-localization, which has important applications in smart city management (Al Nuaimi et al. 2015; Hong et al. 2021), disaster monitoring (Hänsch et al. 2022; Zhang and Wang 2024), autonomous driving (Häne et al. 2017) and so on. A straightforward scheme is to imitate cross-view image geo-localization (Workman, Souvenir, and Jacobs 2015; Hu et al. 2018; Shi et al. 2019; Yang, Lu, and Zhu 2021; Zhu, Shah, and Chen 2022; Deuser, Habel, and Oswald 2023) using a retrieval-based approach. In this setting, first partition the reference image into uniformly-sized patches and then retrieve the patch most similar to the object of interest as the localization result. However, since objects exhibit diverse shapes and scales, uniformly-sized patches are insufficient to represent objects of arbitrary sizes. Subsequent works (Sun

et al. 2023; Li et al. 2025) adopt anchor-based scheme. They adjust a set of predefined anchors with different aspect ratios and select the box that best matches the object as the localization result. This scheme addresses the uniformly-patch limitation.

However, anchor-based paradigm relies on anchors that are manually designed or obtained by clustering. Such anchors neither accurately describe object sizes nor avoid introducing complex hyperparameter tuning and bulky detection heads (Tian et al. 2019; Kong et al. 2020). To the best of our knowledge, we are the first to propose an anchor-free localization scheme to overcome these issues in cross-view object geo-localization. In our anchor-free scheme, we draw inspiration from the object detection methodology of FCOS (Tian et al. 2019) and directly predict the offsets from each pixel to the object in four directions (left, right, top, bottom), thereby eliminating reliance on prior boxes. Our approach inherits the advantages of anchor-free architectures, including: (1) elimination of dependence on candidate anchors (Tian et al. 2019), leading to reduced computational cost; (2) reduction in the need for hyperparameter tuning (Tian et al. 2019; Kong et al. 2020), improving generalization capability; (3) capability to directly predict object locations, enabling more flexible adaptation to objects of different scales. Different cross-view object geo-localization schemes are illustrated in Fig. 1 (b).

Despite the merits of anchor-free schemes, cross-view object geo-localization remains challenging. A click point in the query image generally corresponds to an uncertain and spatially dispersed region in the reference image due to projection geometry or annotation imprecision, which makes the task particularly difficult. In addition, owing to the substantial viewpoint differences between query and reference images, as well as variations in capture conditions such as time, illumination, blur, and occlusion, the same object can exhibit significant geometric and appearance discrepancies across views, further complicating cross-view object localization.

To address these challenges, we propose a novel anchor-free cross-view object geo-localization framework. The framework employs a new Gaussian Position Encoding (GPE) that represents the click point in the query image as the center of a 2D Gaussian distribution and uses a learnable standard deviation to adaptively adjust the encoding ex-

*Corresponding author.

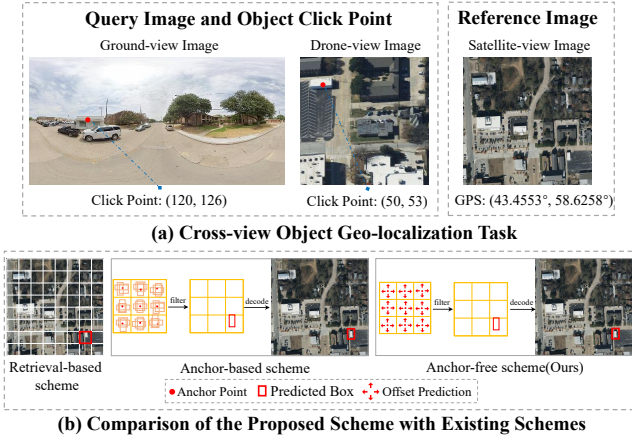


Figure 1: Illustration of the cross-view object geo-localization task and comparison of different solutions. **(a)** The reference image is usually a satellite image with geographic information (a GPS coordinate). The query image is from a ground or drone view, with the click point (red dots) of the object of interest. Cross-view object geo-localization aims to find the geographic location of an object of interest in a query image from a reference image with attached geographic information. **(b)** The retrieval-based scheme divides the satellite image into uniformly-sized patches to construct a reference database and attempts to retrieve the patch that is most semantically similar to the object of interest as a location proposal. The anchor-based scheme generates a series of candidate bounding boxes for each anchor based on predefined anchors, and then selects the best bounding box containing the object of interest from these candidates. The anchor-free (ours) scheme directly predicts the object location at each pixel and selects the best bounding box containing the object of interest. Obviously, our scheme is no longer constrained by predefined anchors.

tent, thereby better accommodating positional uncertainty. In addition, the framework integrates a Cross-view Object Association Module (CVOAM), which associates consistent semantics of the same object and its surrounding context across views via interaction between the module’s two network branches, thereby improving cross-view localization capability. Notably, the two main components of our framework, GPE and CVOAM, introduce no additional parameter overhead (except for the learnable standard deviation in GPE), which contributes to the lightweight nature of the model. The main contributions of this paper are as follows:

- We first adopt an anchor-free localization paradigm for cross-view object geo-localization. We propose an end-to-end anchor-free cross-view object geo-localization network (AFGeo) that eliminates reliance on candidate anchors, improving flexibility and generalization capability for cross-view object matching.
- To provide a more robust positional prior, we introduce a novel Gaussian Position Encoding (GPE) that models object location uncertainty as a smooth probability distribution. We also propose a Cross-view Object Associ-

ation Module (CVOAM) to associate consistent object semantics across views and improve localization performance. Notably, GPE and CVOAM introduce negligible—or even no—additional parameters and contribute to the lightweight design.

- Extensive experiments on the CVOGL (Sun et al. 2023) benchmark and G2D demonstrate that our AFGeo surpasses current state-of-the-art methods, significantly improving localization accuracy while maintaining a compact model size. Our method offers an effective solution for deploying object-level geo-localization in real-world systems with limited computational resources.

Related Work

Retrieval-based Cross-view Object Geo-localization. A natural idea for cross-view object geo-localization is to adapt retrieval-based strategies from cross-view image geo-localization (Hu et al. 2018; Lin et al. 2022; Yang, Lu, and Zhu 2021; Shi et al. 2019; Zhu, Shah, and Chen 2022; Deuser, Habel, and Oswald 2023; Mi et al. 2025). In this setting, the satellite reference image is divided into a set of uniformly sized patches, and each patch is treated as a candidate location. The model extracts feature embeddings for both the query object and all reference patches, and the patch with the highest similarity score is selected as the predicted object location. Although conceptually simple, patch retrieval suffers from several drawbacks. The spatial resolution of localization is inherently limited by the patch granularity, making it difficult to achieve precise bounding box alignment. The exhaustive comparison across all patches also introduces high computational cost for large-scale reference images. These limitations have motivated research into alternative solutions.

Anchor-based Cross-view Object Geo-localization. Inspired by advances in object detection, several works (Sun et al. 2023; Li et al. 2025) adopt anchor-based mechanisms for cross-view object localization. These methods generate a large set of predefined anchor boxes in the reference image and then predict classification and regression offsets to identify the target object. While anchor-based strategies achieve better localization accuracy than retrieval-based methods, they suffer from several intrinsic drawbacks. First, detection performance is highly sensitive to the predefined anchor hyperparameters (e.g., sizes, aspect ratios, and numbers), which require extensive heuristic tuning. Second, the fixed design of anchor boxes limits their ability to generalize across objects of varying scales and aspect ratios, particularly in challenging cross-view scenarios. Moreover, dense placement of anchors introduces a massive number of negative samples, leading to severe class imbalance and increased computational overhead. Finally, anchor-based approaches involve additional complexity from IoU computations and anchor-to-ground-truth matching during training.

Anchor-free Cross-view Object Geo-localization. Recently, anchor-free approaches (Tian et al. 2019; Law and Deng 2018; Duan et al. 2019; Zhou, Zhuo, and Krahenbuhl 2019; Kong et al. 2020) in object detection have emerged as a promising alternative by eliminating the dependency on

predefined anchors. These methods completely sidestep the need for heuristic tuning of hyperparameters related to anchor shapes, sizes, and ratios, which are often critically sensitive to detection accuracy. In this paper, we first adopt an anchor-free paradigm for cross-view object geo-localization. This innovative methodology inherits the intrinsic advantages of anchor-free paradigms, exploring novel possibilities and opening up new avenues for the task of cross-view object geo-localization.

Position Encoding & Cross-view Fusion. Sun et al. (2023) propose a positional encoding method based on the Euclidean distance from each spatial location to the click point, generating a spatial weight matrix that highlights the approximate area around the query object. This positional prior is concatenated with the query image features and processed through a cross-view fusion module equipped with spatial attention, which enhances the feature discriminability in the reference image by focusing on regions most relevant to the query. Li et al. (2025) introduce a view-specific positional encoding (VSPE) strategy that differentiates between ground and drone views. They further improved feature representation through a channel-spatial hybrid attention (CSHA) mechanism. Unlike these methods, our proposed Gaussian Position Encoding (GPE) represents a significant advancement in handling positional uncertainty and adaptive context modeling. Moreover, we develop the Cross-view Object Association Module (CVOAM), which goes beyond conventional fusion mechanisms by explicitly associating consistent object semantics across views.

Methodology

The overview of our proposed AFGeo model is shown in Fig. 2. The AFGeo architecture mainly consists of Gaussian Position Encoding (GPE), the Cross-View Object Association Module (CVOAM), and an object localization head that adopts the anchor-free paradigm. We will elaborate on the key components in the following sections.

Gaussian Position Encoding

In cross-view object geo-localization, position encoding serves as an effective spatial prior to guide feature extraction and object localization. We observe that the click point and its vicinity contain rich object semantic information. Therefore, reasonable modeling of the click point is crucial for the subsequent task of locating the object in the reference image. In this paper, we model the click point by using Gaussian Position Encoding (GPE), as shown in Eq. 1.

$$P_k(i, j) = \exp \left(-\frac{(||z_k(i, j) - p_k||_2)^2}{2\sigma^2} \right) \quad (1)$$

where $P_k(i, j)$ denotes the encoding of the click point of the k -th sample at the i -th row and j -th column, $z_k(i, j)$ denotes the pixel position at the i -th row and j -th column of the k -th sample, p_k denotes the click point of the object of interest, σ denotes the standard deviation. Compared to the Euclidean or hybrid Euclidean distance position encodings in (Sun et al. 2023; Li et al. 2025), we introduce a learnable standard deviation σ in GPE to adaptively control the encoding range. This enables the model to produce a concentrated

distribution for small objects and a broader distribution for large objects (as shown in Fig. 3), providing a more robust spatial prior. Notably, GPE adds only a single σ parameter, imposing negligible overhead on the overall model.

Cross-view Object Association Module

Human perception offers a crucial insight: when establishing cross-view object associations, observers naturally integrate target objects with their semantic context (e.g., road structure, surrounding buildings). This cognitive behavior indicates that reliable object matching inherently depends on the semantic consistency of the local environment—a critical signal overlooked by existing methods. Current approaches (Deuser, Habel, and Oswald 2023; Sun et al. 2023; Li et al. 2025) compress image feature maps into a single global query vector, which overemphasizes holistic representations and results in the loss of fine-grained details. To address this limitation, we introduce a Cross-View Object Association Module (CVOAM) that enables the model to automatically focus on both critical local features and global contextual cues for robust cross-view object matching.

CVOAM consists of two parallel sub-networks that fuse the feature outputs of the query branch $\mathbf{F}_q \in \mathbb{R}^{H_1 \times W_1 \times C}$ and the reference branch $\mathbf{F}_r \in \mathbb{R}^{H_2 \times W_2 \times C}$. In the first sub-network (blue background in Fig. 2), \mathbf{F}_q is globally average-pooled over the spatial dimensions and multiplied with raw \mathbf{F}_r to produce a weight matrix $\mathbf{A}_1 \in \mathbb{R}^{H_2 \times W_2}$. \mathbf{A}_1 is then applied to raw \mathbf{F}_r , yielding the sub-network output $\mathbf{O}_1 \in \mathbb{R}^{H_2 \times W_2 \times C}$.

$$\mathbf{F}_q = \frac{1}{H_1 \times W_1} \sum_{i=1}^{H_1} \sum_{j=1}^{W_1} \mathbf{F}_q[i, j, :] \quad (2)$$

$$\mathbf{A}_1 = \text{Normalize}(\mathbf{F}_r \cdot \mathbf{F}_q^T) \quad (3)$$

$$\mathbf{O}_1 = \mathbf{A}_1 \odot \mathbf{F}_r \quad (4)$$

Where \odot denotes element-wise multiplication. Then, in the second sub-network (green background in Fig. 2), \mathbf{F}_q is globally average-pooled over the channel dimensions, upsampled, reshaped and multiplied with reshaped \mathbf{F}_r to produce a weight matrix $\mathbf{A}_2 \in \mathbb{R}^{1 \times C}$. \mathbf{A}_2 is then applied to raw \mathbf{F}_r , yielding the sub-network output $\mathbf{O}_2 \in \mathbb{R}^{H_2 \times W_2 \times C}$.

$$\mathbf{F}_q = \text{Reshape}(\text{Upsample}(\frac{1}{C} \sum_{i=1}^C \mathbf{F}_q[:, :, i])) \quad (5)$$

$$\mathbf{A}_2 = \text{Reshape}(\text{Normalize}(\mathbf{F}_q \cdot \text{Reshape}(\mathbf{F}_r))) \quad (6)$$

$$\mathbf{O}_2 = \mathbf{A}_2 \odot \mathbf{F}_r \quad (7)$$

Also, \odot denotes element-wise multiplication. Finally, the outputs of the two sub-networks are aggregated by element-wise addition to yield the fused representation $\mathbf{O}_{\text{fusion}} = \mathbf{O}_1 + \mathbf{O}_2$. CVOAM introduces no additional parameters to the model, maintaining the efficiency and compactness of the overall model.

Anchor-free Localization Head

We decouple classification and regression in the anchor-free localization head. The classification branch outputs a tensor $\hat{\mathbf{C}} \in \mathbb{R}^{H \times W \times 1}$, where $\hat{c}_{x,y}$ denotes the targetness logit

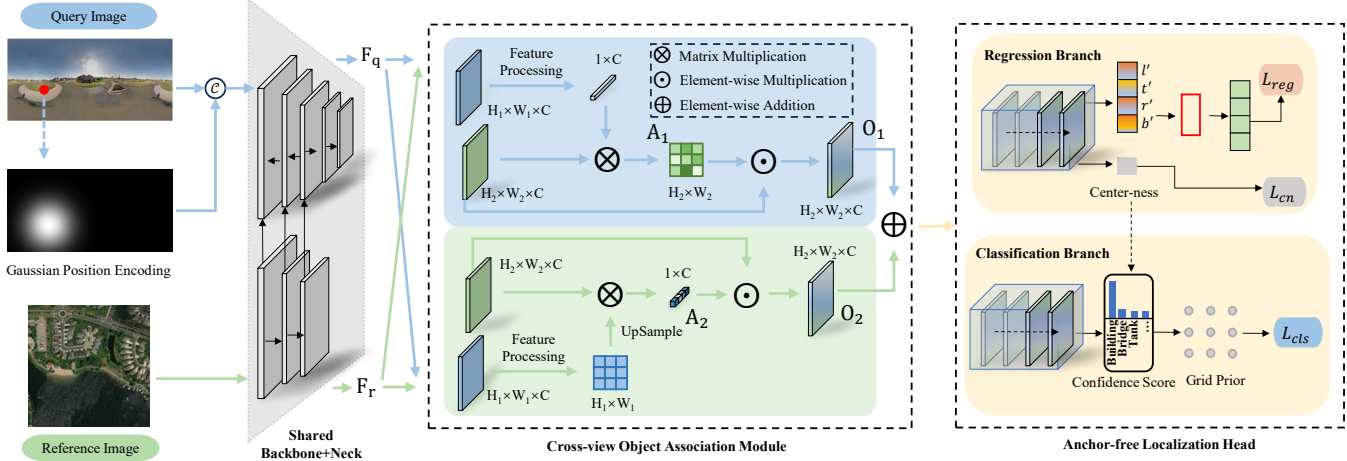


Figure 2: Overview of our AFGeo. AFGeo adopts an anchor-free architecture for cross-view object geo-localization. The structure consists of two key components: Gaussian Position Encoding and the Cross-View Object Association Module, with the localization head following the anchor-free paradigm.

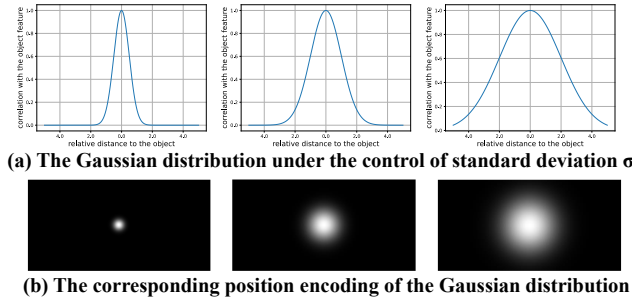


Figure 3: Illustration of the proposed GPE. **(a)** We employ a learnable standard deviation to control the Gaussian distribution, enabling the model to adaptively learn the relationship between the relative distance of the object and the correlation of object features, meaning that the farther the relative distance, the weaker the feature correlation. **(b)** We visualize the position encodings under different Gaussian distributions. The learnable GPE allows the model to better adapt to the uncertainty of object locations, focusing more on the object feature regions (gray-white areas) while ignoring the interference from irrelevant background (black areas).

at location (x, y) . Here, the channel dimension is set to 1, as our task focuses on localizing a common foreground object across cross-view images. The regression branch outputs $\hat{\mathbf{S}} \in \mathbb{R}^{H \times W \times 1}$ and $\hat{\mathbf{B}} \in \mathbb{R}^{H \times W \times 4}$. $\hat{s}_{x,y}$ indicates the estimated centerness at location (x, y) , which helps suppress low-quality predictions far from the actual object center. $\hat{b}_{x,y} = (\hat{l}, \hat{t}, \hat{r}, \hat{b})$ denotes the predicted distances from location (x, y) to four boundaries of the ground-truth (GT) box.

Training. Our label assignment strategy follows (Tian et al. 2019). A feature location (x, y) is assigned as positive if it satisfies two criteria: (1) it lies inside a GT box and falls within a disk of radius ρ centered at the GT box center,

and (2) the predicted object size falls into the scale range handled by the current feature level. If a location falls into multiple GT boxes, we simply assign it to the smallest-area box. For a positive location, the targets are $c_{x,y}^* = 1$, $b_{x,y}^* = (l^*, t^*, r^*, b^*)$ and $s_{x,y}^* = \sqrt{\frac{\min(l^*, r^*)}{\max(l^*, r^*)} \times \frac{\min(t^*, b^*)}{\max(t^*, b^*)}}$, where l^*, t^*, r^* and b^* are the ground-truth distances from location (x, y) to the ground-truth (GT) box. Locations that do not satisfy the conditions are labeled negative with $c_{x,y}^* = 0$.

Inference. During inference, the final detection confidence at each location is obtained by multiplying the classification score and the centerness score. The bounding box prediction corresponding to the location with the highest combined confidence is selected as the final output.

Loss Function

Our training loss function is defined as follows:

$$\begin{aligned} \mathcal{L} = & \frac{\lambda_{cls}}{N_{pos}} \sum_{x,y} \mathcal{L}_{cls}(\hat{c}_{x,y}, c_{x,y}^*) \\ & + \frac{\lambda_{cn}}{N_{pos}} \sum_{x,y} \mathbb{1}_{\{c_{x,y}^* > 0\}} \mathcal{L}_{cn}(\hat{s}_{x,y}, s_{x,y}^*) \\ & + \frac{\lambda_{reg}}{N_{pos}} \sum_{x,y} \mathbb{1}_{\{c_{x,y}^* > 0\}} \mathcal{L}_{reg}(\hat{b}_{x,y}, b_{x,y}^*) \end{aligned} \quad (8)$$

Where \mathcal{L}_{cls} is focal loss as in (Lin et al. 2017), \mathcal{L}_{cn} is Binary Cross-Entropy (BCE) loss as in (Goodfellow et al. 2016) and \mathcal{L}_{reg} is GIoU loss as in (Rezatofighi et al. 2019). $\mathbb{1}_{\{c_{x,y}^* > 0\}}$ is the indicator function, being 1 if $c_{x,y}^* > 0$ and 0 otherwise. λ_{cls} , λ_{cn} and λ_{reg} are balance weights and are set to 1 in this paper. N_{pos} denotes the number of positive samples.

Experiment

Dataset and Evaluation Metrics

CVOGL Dataset. CVOGL consists of two types of cross-view object geo-localization tasks: Task 1 (Ground → Satel-

| Method | Ground→Satellite | | | | Drone→Satellite | | | |
|-------------|------------------|----------------|-----------------|----------------|-----------------|----------------|-----------------|----------------|
| | Test | | Validation | | Test | | Validation | |
| | acc@ 0.25(%) | acc@ 0.5(%) | acc@ 0.25(%) | acc@ 0.5(%) | acc@ 0.25(%) | acc@ 0.5(%) | acc@ 0.25(%) | acc@ 0.5(%) |
| CVM-Net | 4.73 | 0.51 | 5.09 | 0.87 | 20.14 | 3.29 | 20.04 | 3.47 |
| RK-Net | 7.40 | 0.82 | 8.67 | 0.98 | 19.22 | 2.67 | 19.94 | 3.03 |
| L2LTR | 10.69 | 2.16 | 12.24 | 1.84 | 38.95 | 6.27 | 38.68 | 5.96 |
| Polar-SAFA | 20.66 | 3.19 | 19.18 | 2.71 | 37.41 | 6.58 | 36.19 | 6.39 |
| TransGeo | 21.17 | 2.88 | 21.67 | 3.25 | 35.05 | 6.37 | 34.78 | 5.42 |
| SAFA | 22.20 | 3.08 | 20.59 | 3.25 | 37.41 | 6.58 | 36.19 | 6.39 |
| Sample4Geo | 5.75 | 1.21 | 6.18 | 0.56 | 6.75 | 1.61 | 7.04 | 1.08 |
| ConGeo | 30.27 | 5.52 | 29.59 | 5.09 | 34.94 | 6.66 | 30.60 | 5.60 |
| DetGeo | 45.43 | 42.24 | 46.70 | 43.99 | 61.97 | 57.66 | 59.81 | 55.15 |
| VAGeo | 47.38 | 43.68 | 47.13 | 43.88 | 58.79 | 54.98 | 56.66 | 52.55 |
| AFGeo(Ours) | 52.31 | 49.64 | 52.87 | 48.65 | 66.29 | 63.10 | 64.68 | 59.70 |

Table 1: Evaluation on CVOGL. Suboptimal results are underlined and best results are shown in bold.

| Method | Ground→Drone | | | |
|-------------|-----------------|----------------|-----------------|----------------|
| | Test | | Validation | |
| | acc@ 0.25(%) | acc@ 0.5(%) | acc@ 0.25(%) | acc@ 0.5(%) |
| RK-Net | 13.84 | 1.47 | 12.85 | 1.58 |
| L2LTR | 19.35 | 3.81 | 18.57 | 3.61 |
| TransGeo | 27.02 | 4.48 | 28.12 | 7.23 |
| Sample4Geo | 48.70 | 7.49 | 54.91 | 8.26 |
| ConGeo | 63.83 | 11.44 | 68.29 | 9.72 |
| DetGeo | 74.59 | 63.51 | 68.29 | 59.95 |
| VAGeo | 76.49 | 72.97 | 74.31 | 68.75 |
| AFGeo(Ours) | 78.65 | 74.86 | 74.54 | 69.68 |

Table 2: Evaluation on G2D. Suboptimal results are underlined and best results are shown in bold.

lite), where ground-view images are used as queries and satellite images as references; and Task 2 (Drone → Satellite), where drone images are used as queries and satellite images as references. The object of interest in a query image is indicated by a clicked point, while the corresponding object in the reference image is annotated with a bounding box. CVOGL contains 6,239 query-reference pairs for each task, with 4,343 for training, 923 for validation, and 973 for testing.

G2D Dataset. G2D is constructed for Ground-to-Drone cross-view object geo-localization by leveraging images from the CVOGL dataset. Ground images are used as queries and drone images as references. G2D contains 2753 query-reference pairs for each task, with 1951 for training, 432 for validation, and 370 for testing.

Implementation Details

We employ pre-trained ResNet-50 as the shared backbone for the two branches. The model is optimized using SGD

with an initial learning rate of 0.01 and trained for 40 epochs on NVIDIA A100 GPUs.

Comparative Experiment

We compare our method with the current state-of-the-art methods on CVOGL and G2D. The experimental results are shown in Table 1 and Table 2. Note that the authors of VAGeo (Li et al. 2025) have not released the source code and the results reported in the table are reproduced by us based on the descriptions in the original paper. According to Table 1 and Table 2, our method achieves significant gains on both Ground→Satellite, Drone→Satellite and Ground→Drone object localization tasks. Notably, under the more challenging Ground→Satellite setting with severe viewpoint changes, our approach improves acc@0.5 by 13.64% on the test set and 10.5% on the validation set. These results demonstrate the superiority of our anchor-free design in various cross-view object geo-localization scenarios.

Ablation Study

We conduct an ablation study to assess the contributions of GPE and CVOAM, as shown in Table 3 and Table 4. Removing both yields the worst performance, while adding either module individually improves results. The best performance occurs when both are combined, highlighting the importance of jointly using GPE and CVOAM for robust object geo-localization.

Visual Analysis

The heatmaps in Fig. 4 illustrate the effectiveness of our method across different scenarios. In the Ground→Satellite scenario, the Baseline (our framework without GPE and CV-PAM) incorrectly attends to irrelevant regions such as roads and forests, whereas AFGeo accurately highlights the query object—the football field—along with its adjacent contextual structures, including semantically related areas such as tennis and baseball courts. In the Ground→Drone scenario,

| GPE | CVOAM | Ground→Satellite | | | | Drone→Satellite | | | |
|-----|-------|------------------|----------------|-----------------|----------------|-----------------|----------------|-----------------|----------------|
| | | Test | | Validation | | Test | | Validation | |
| | | acc@ 0.25(%) | acc@ 0.5(%) | acc@ 0.25(%) | acc@ 0.5(%) | acc@ 0.25(%) | acc@ 0.5(%) | acc@ 0.25(%) | acc@ 0.5(%) |
| ✗ | ✗ | 49.64 | 47.28 | 48.00 | 44.85 | 51.59 | 49.33 | 47.35 | 43.88 |
| ✓ | ✗ | 51.90 | 49.33 | 48.75 | 45.40 | 52.93 | 51.18 | 50.16 | 46.80 |
| ✗ | ✓ | 50.98 | 48.10 | 52.33 | 48.00 | 65.70 | 62.28 | 61.65 | 57.85 |
| ✓ | ✓ | 52.31 | 49.64 | 52.87 | 48.65 | 66.29 | 63.10 | 64.68 | 59.70 |

Table 3: Ablation for GPE and CVOAM on CVOGL. Best results are shown in bold.

| GPE | CVOAM | Ground→Drone | | | |
|-----|-------|-----------------|----------------|-----------------|----------------|
| | | Test | | Validation | |
| | | acc@ 0.25(%) | acc@ 0.5(%) | acc@ 0.25(%) | acc@ 0.5(%) |
| ✗ | ✗ | 74.01 | 69.68 | 70.81 | 65.15 |
| ✓ | ✗ | 76.49 | 72.97 | 72.84 | 68.15 |
| ✗ | ✓ | 77.84 | 73.32 | 73.48 | 69.44 |
| ✓ | ✓ | 78.65 | 74.86 | 74.54 | 69.68 |

Table 4: Ablation for GPE and CVOAM on G2D. Best results are shown in bold.

although the Baseline captures the queried building, it also overemphasizes several visually similar buildings, while our method mitigates such distractions and maintains focus on the true target. In the Drone→Satellite scenario, the Baseline fails to locate the correct building, whereas our method successfully identifies the target. These observations demonstrate that the proposed GPE and CVPAM not only guide the model to accurately attend to the query object but also exploit its surrounding semantically consistent context across views, thereby improving both the robustness and accuracy of object localization. Furthermore, Fig. 5 presents qualitative results under different cross-view scenarios, where the high overlap between the predicted and ground-truth bounding boxes highlights the precise localization performance achieved by our AFGeo.

Conclusion

We first introduce an anchor-free architecture in cross-view object geo-localization (AFGeo), incorporating GPE to provide a more robust positional prior and CVOAM to associate consistent object semantics across views, thereby jointly enhancing localization performance. AFGeo is a lightweight and efficient model structure, and we hope this work can serve as a reference for deploying cross-view object geo-localization systems in resource-constrained environments.

References

Al Nuaimi, E.; Al Neyadi, H.; Mohamed, N.; and Al-Jaroodi, J. 2015. Applications of big data to smart cities. *Journal of Internet Services and Applications*, 6(1): 1–15.

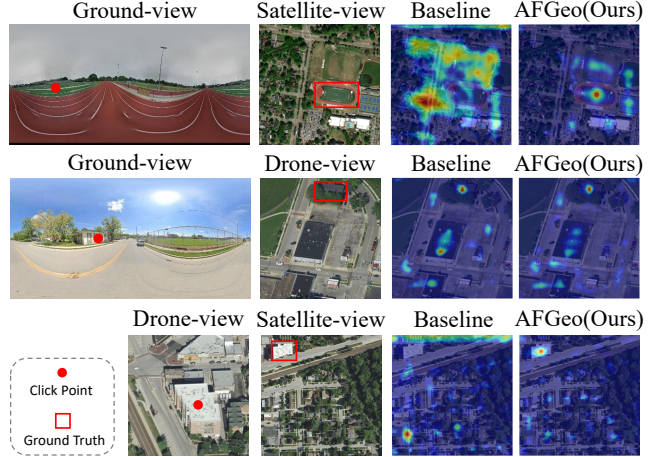


Figure 4: Heatmap visualization of Baseline (our framework without GPE and CVPAM) and the proposed AFGeo. The red dot denotes the click point and the red box denotes the ground-truth bounding box.

Deuser, F.; Habel, K.; and Oswald, N. 2023. Sample4geo: Hard negative sampling for cross-view geo-localisation. In *Proceedings of the IEEE/CVF International Conference on Computer Vision*, 16847–16856.

Duan, K.; Bai, S.; Xie, L.; Qi, H.; Huang, Q.; and Tian, Q. 2019. Centernet: Keypoint triplets for object detection. In *Proceedings of the IEEE/CVF international conference on computer vision*, 6569–6578.

Goodfellow, I.; Bengio, Y.; Courville, A.; and Bengio, Y. 2016. *Deep learning*, volume 1. MIT Press.

Häne, C.; Heng, L.; Lee, G. H.; Fraundorfer, F.; Furgale, P.; Sattler, T.; and Pollefeys, M. 2017. 3D visual perception for self-driving cars using a multi-camera system: Calibration, mapping, localization, and obstacle detection. *Image and Vision Computing*, 68: 14–27.

Hänsch, R.; Arndt, J.; Lunga, D.; Gibb, M.; Pedelose, T.; Boedihardjo, A.; Petrie, D.; and Bacastow, T. M. 2022. Spacenet 8—the detection of flooded roads and buildings. In *Proceedings of the IEEE/CVF conference on computer vision and pattern recognition*, 1472–1480.

Hong, D.; Hu, J.; Yao, J.; Chanussot, J.; and Zhu, X. X. 2021. Multimodal remote sensing benchmark datasets for

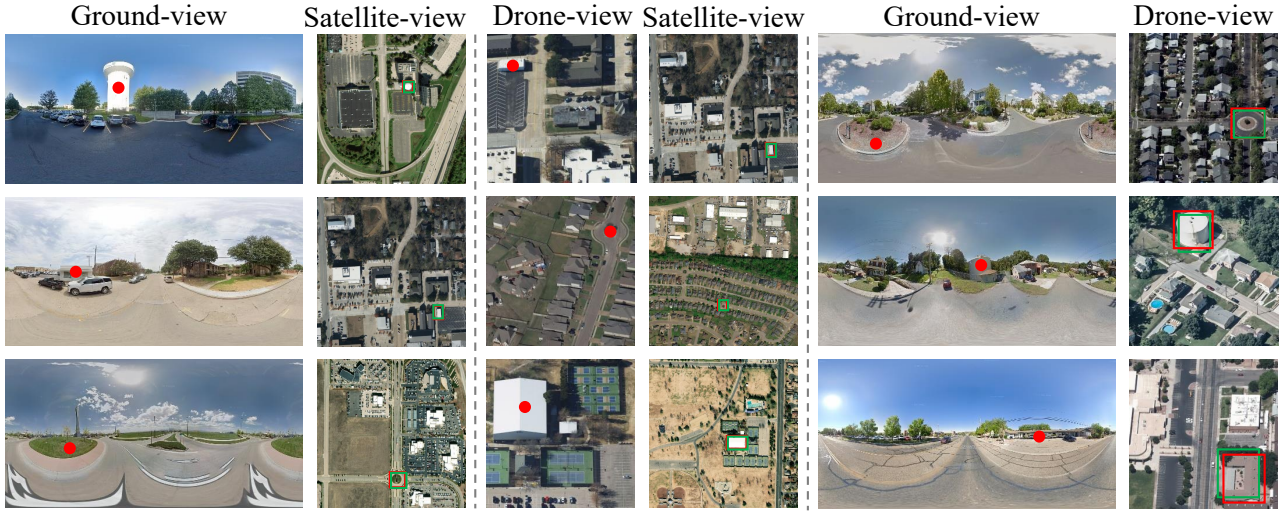


Figure 5: Object localization results by our AFGeo. The red and green bounding boxes denote the ground-truth and predicted results, respectively.

land cover classification with a shared and specific feature learning model. *ISPRS Journal of Photogrammetry and Remote Sensing*, 178: 68–80.

Hu, S.; Feng, M.; Nguyen, R. M.; and Lee, G. H. 2018. Cvm-net: Cross-view matching network for image-based ground-to-aerial geo-localization. In *Proceedings of the IEEE Conference on Computer Vision and Pattern Recognition*, 7258–7267.

Kong, T.; Sun, F.; Liu, H.; Jiang, Y.; Li, L.; and Shi, J. 2020. Foveabox: Beyond anchor-based object detection. *IEEE Transactions on Image Processing*, 29: 7389–7398.

Law, H.; and Deng, J. 2018. CornerNet: Detecting objects as paired keypoints. In *Proceedings of the European conference on computer vision (ECCV)*, 734–750.

Li, Z.; Yuan, X.; Liu, W.; and Xu, X. 2025. VAGeo: View-specific Attention for Cross-View Object Geo-Localization. In *ICASSP 2025 - 2025 IEEE International Conference on Acoustics, Speech and Signal Processing (ICASSP)*, 1–5.

Lin, J.; Zheng, Z.; Zhong, Z.; Luo, Z.; Li, S.; Yang, Y.; and Sebe, N. 2022. Joint representation learning and keypoint detection for cross-view geo-localization. *IEEE Transactions on Image Processing*, 31: 3780–3792.

Lin, T.-Y.; Goyal, P.; Girshick, R.; He, K.; and Dollár, P. 2017. Focal loss for dense object detection. In *Proceedings of the IEEE international conference on computer vision*, 2980–2988.

Mi, L.; Xu, C.; Castillo-Navarro, J.; Montariol, S.; Yang, W.; Bosselut, A.; and Tuia, D. 2025. ConGeo: Robust Cross-View Geo-Localization Across Ground View Variations. In Leonardis, A.; Ricci, E.; Roth, S.; Russakovsky, O.; Sattler, T.; and Varol, G., eds., *Computer Vision – ECCV 2024*, 214–230. Cham: Springer Nature Switzerland. ISBN 978-3-031-72630-9.

Rezatofighi, H.; Tsoi, N.; Gwak, J.; Sadeghian, A.; Reid, I.; and Savarese, S. 2019. Generalized intersection over union:

A metric and a loss for bounding box regression. In *Proceedings of the IEEE/CVF conference on computer vision and pattern recognition*, 658–666.

Shi, Y.; Liu, L.; Yu, X.; and Li, H. 2019. Spatial-aware feature aggregation for image based cross-view geo-localization. *Advances in Neural Information Processing Systems*, 32.

Sun, Y.; Ye, Y.; Kang, J.; Fernández-Beltran, R.; Feng, S.; Li, X.; Luo, C.; Zhang, P.; and Plaza, A. 2023. Cross-View Object Geo-Localization in a Local Region With Satellite Imagery. *IEEE Trans. Geosci. Remote. Sens.*, 61: 1–16.

Tian, Z.; Shen, C.; Chen, H.; and He, T. 2019. Fcos: Fully convolutional one-stage object detection. In *Proceedings of the IEEE/CVF international conference on computer vision*, 9627–9636.

Workman, S.; Souvenir, R.; and Jacobs, N. 2015. Wide-area image geolocalization with aerial reference imagery. In *Proceedings of the IEEE International Conference on Computer Vision*, 3961–3969.

Yang, H.; Lu, X.; and Zhu, Y. 2021. Cross-view geo-localization with layer-to-layer transformer. *Advances in Neural Information Processing Systems*, 34: 29009–29020.

Zhang, C.; and Wang, S. 2024. Good at captioning bad at counting: Benchmarking gpt-4v on earth observation data. In *Proceedings of the IEEE/CVF Conference on Computer Vision and Pattern Recognition*, 7839–7849.

Zhou, X.; Zhuo, J.; and Krahenbuhl, P. 2019. Bottom-up object detection by grouping extreme and center points. In *Proceedings of the IEEE/CVF conference on computer vision and pattern recognition*, 850–859.

Zhu, S.; Shah, M.; and Chen, C. 2022. Transgeo: Transformer is all you need for cross-view image geo-localization. In *Proceedings of the IEEE/CVF Conference on Computer Vision and Pattern Recognition*, 1162–1171.